Ukrainian Journal of Physical Optics
ISSUE 2
2024

OPTICAL VORTICES GENERATED IN MULTI-CASCADE OPTICAL SYSTEMS WITH TORSION-STRESSED $LiNbO_3$ CRYSTALLINE ELEMENTS

D. ADAMENKO, T. KRYVYY, I. SKAB, AND R. VLOKH

O. G. Vlokh Institute of Physical Optics, 23 Dragomanov Str., 79005, Lviv, Ukraine,
vlokh@ifo.lviv.ua

Received: 26.03.2024

Abstract. This work theoretically tested the possibility of expanding the spectrum of vortex charges generated using multi-cascade optical systems based on $LiNbO_3$ crystals twisted around their optical axis. As a result, analytical expressions for the electric field parameters of the output optical wave were obtained for the four main types of elementary cascades that allow the generation of vortices with charges +1 and −1 and also provide the matching of adjacent cascades in the multi-cascade optical system. At the same time, it was shown that when using the appropriate number of sequentially located cascades, each of which belongs to a certain type from the above, it is possible to generate a vortex beam with arbitrary integer vortex charges, including zero. Using the proposed cascade system, one can operate the outgoing beam parameters. This system can be used at the vortex beam multiplexing for information transfer.

Keywords: optical vortex, helical wavefront, vortex charge, multi-cascade optical system, torsion stresses, $LiNbO_3$ crystals
UDC: 535.551
DOI: 10.3116/16091833/Ukr.J.Phys.Opt.2024.02099

1. Introduction

Using composite vortex beams increases the data transfer rate to hundreds of Gbit/s [1] and, with multiplexing and demultiplexing, to several Tbit/s [2]. Therefore, in the last few years, considerable attention has been devoted to searching for opportunities to generate composite vortex beams, their modulation and demodulation, and multiplexing and demultiplexing. In particular, in the work [3], the possibility of generation and modulation-demodulation of optical vortex beams with different charges using a spatial light modulator with a loaded complex hologram was demonstrated. A liquid crystal spatial light modulator was used to form vector-vortex beams, as well as a laser with applied concentric rings on the resonator mirror [4-6]. The work [7] was devoted to the problem of generating optical vortex beams and their multiplexing and demultiplexing. The obtained results demonstrated uninterrupted transmission of information. However, the above generation, modulation, and multiplexing methods of composite beams require high-technologies. In addition, most of these devices are passive, using pre-made optical elements that cannot change their parameters.

Let us review the main methods of generation of optical vortices. Optical vortices can be generated using various experimental methods and media, including the diffraction method on computer-synthesized forked holograms [8], spiral phase plates [9], *q*-plates [10], crystal optical method using divergent incident beam [11], nanoscale metasurfaces [12], spatial light modulators [13], etc. Today, one of the main methods of generating optical vortices is the use

of the so-called q-plate – a linear phase plate retarder with a phase delay of π, where the main axis of the retarder repeats q times the azimuthal angle φ [14]. These q-plates are characterized by the strength of the topological defect of director orientation q and generate an optical vortex with an orbital angular momentum (charge) equal to l=2q [15].

Another fairly promising method of generating optical vortices is using anisotropic inhomogeneous media under certain external influences [16-18] – particularly, a crystalline sample mechanically twisted around a certain crystallographic direction. Thus, in particular, in work [19], it was experimentally established and confirmed by theoretical calculations that when an initially Gaussian beam propagates in an optical system consisting of a right circular polarizer, a uniaxial LiNbO3 crystal twisted around its optical axis and a left circular polarizer, an optical vortex with a unitary topological charge appears. In turn, work [20] theoretically demonstrated that the output optical beam emerging from the optical system consisting of a right circular polarizer, cubic KAl(SO4)2×12H2O crystals twisted around the [111] direction, and a left circular polarizer should bear a single-charged optical vortex. However, in the above work, the parameters of the output optical waves were calculated using only numerical methods.

Testing of the assumption that using several devices for generating optical vortices in an optical system under certain conditions can lead to a significant expansion of the spectrum of charges of generated vortices has been carried out for q-plates in work [14]. This work has implemented approaches to add, subtract, or change the sign of commercially available q-plates with topological strength of defect equal to 1/2 and 1, which involve various combinations of q-plates with half-wave plates in optical systems equivalent to a certain single q-plate. As a result, it has been theoretically shown that for these optical systems using collimated incident beam and N q-plates with different topological strengths of defect, it is possible to obtain 3^N different combinations of q values. On the other hand, one can assume a similar effect by using torsion-stressed crystalline elements. However, the torsion-stressed crystalline rods differ from the q-plates in terms of the linear radial distribution of the phase difference, which can be operated by the applied torque moment. Such a distribution does not characterize the q-plates, while the phase difference in these plates can only be fine-tuned by the applied bias field [21]. Thus, in the presented work, we will analyze the overall properties of multi-cascade optical systems with torsion-stressed $LiNbO_3$ crystalline elements placed in them and demonstrate their arithmetic properties in generating optical vortices and composite vortex beams.

2. Method of analysis

Consider a cylindrical sample with length d and radius R made of a $LiNbO_3$ crystal belonging to the point symmetry group 3m. Its axis coincides with the optical axis of this crystal and the x_3 axis. The basis vectors of coordinate system $x_1x_2x_3$ coincide with eigenvectors of the dielectric impermeability tensor. If the torque moment M is applied to the ends of this cylindrical sample, and its side surface is free of loads, the following nonzero components of the mechanical stress tensor (second rank polar tensor with internal symmetry [V^2]) appear as a result [22]:

$$\sigma_{32}=\sigma_{23}=\frac{2M}{\pi R^4}r\cos\varphi\,,\ \sigma_{31}=\sigma_{13}=\frac{2M}{\pi R^4}r\sin\varphi\,, \tag{1}$$

where r and φ represent, respectively, the radial and azimuthal coordinates of the polar coordinate system

$$\begin{cases} x_1 = r\cos\varphi \\ x_2 = r\sin\varphi \end{cases}. \tag{2}$$

The presence of non-zero components of the mechanical stress tensor leads to the appearance of the piezo-optical effect described by the relation:

$$\Delta B_{ik} = \pi_{ikts}\sigma_{ts}, \tag{3}$$

where ΔB_{ik} is the piezo-optical contribution to the optical dielectric impermeability (second rank polar tensor with internal symmetry [V²]); π_{ikts} is the piezo-optical tensor (fourth rank polar tensor with internal symmetry [V²]²). Given that the piezo-optical coefficients tensor for the point symmetry group 3m has the form:

π_{ikts}	σ_{11}	σ_{22}	σ_{33}	σ_{23}	σ_{13}	σ_{12}
ΔB_{11}	π_{11}	π_{12}	π_{13}	π_{14}	0	0
ΔB_{22}	π_{12}	π_{11}	π_{13}	$-\pi_{14}$	0	0
ΔB_{33}	π_{31}	π_{31}	π_{33}	0	0	0
ΔB_{23}	π_{41}	$-\pi_{41}$	0	π_{44}	0	0
ΔB_{13}	0	0	0	0	π_{44}	$2\pi_{41}$
ΔB_{12}	0	0	0	0	π_{14}	$\pi_{11}-\pi_{12}$

, (4)

the equation of the optical indicatrix can be written as:

$$\begin{aligned} &((B_{11})_0 + \pi_{14}\sigma_{23})x_1^2 + ((B_{11})_0 - \pi_{14}\sigma_{23})x_2^2 + (B_{33})_0 x_3^2 \\ &+2\pi_{44}\sigma_{23}x_2x_3 + 2\pi_{44}\sigma_{13}x_1x_3 + 2\pi_{14}\sigma_{13}x_1x_2 = 1. \end{aligned} \tag{5}$$

For a cross-section in the plane $x_3 = 0$, Eq. (5) reduces to the form

$$((B_{11})_0 + \pi_{14}\sigma_{23})x_1^2 + ((B_{11})_0 - \pi_{14}\sigma_{23})x_2^2 + 2\pi_{14}\sigma_{13}x_1x_2 = 1. \tag{6}$$

Given that $(B_{11})_0 = 1/n_0^2$, where n_0 is the ordinary refractive index for a non-twisted $LiNbO_3$ crystal, the main refractive indices for a twisted cylindrical $LiNbO_3$ crystalline sample can be found from Eq. (6)

$$n_{1,2} = n_0 \pm 0{,}5n_0^3\pi_{14}(\sigma_{23}^2 + \sigma_{13}^2)^{0,5} = n_0 \pm \frac{Mn_0^3\pi_{14}}{\pi R^4}r. \tag{7}$$

Thus, the birefringence of this twisted sample is equal to:

$$\Delta n = n_1 - n_2 = \frac{2Mn_0^3\pi_{14}}{\pi R^4}r. \tag{8}$$

In turn, the phase delay for this twisted sample can be written as:

$$\Delta\Gamma = 2\pi d\Delta n/\lambda = \frac{4dMn_0^3\pi_{14}}{\lambda R^4}r = 2AMr, \tag{9}$$

where the quantity $A = \frac{2dn_0^3\pi_{14}}{\lambda R^4} = \text{const}$. Finally, the angle of rotation of the optical indicatrix around the x_3 axis is equal to

$$\theta = 0.5\arctan\left(\frac{\sigma_{13}}{\sigma_{23}}\right) = 0.5\arctan\left(\frac{\sin\varphi}{\cos\varphi}\right) = 0.5\varphi. \tag{10}$$

Therefore, using the relationship for the Jones matrix of an arbitrary phase retarder [23]

$$J_{PR}=\left[\begin{array}{c|c}\cos(\Delta\Gamma/2)+i\sin(\Delta\Gamma/2)\cos(2\theta) & i\sin(\Delta\Gamma/2)\sin(2\theta)\\ \hline i\sin(\Delta\Gamma/2)\sin(2\theta) & \cos(\Delta\Gamma/2)-i\sin(\Delta\Gamma/2)\cos(2\theta)\end{array}\right], \qquad (11)$$

it is possible to write down the Jones matrix for a certain unit cell with polar coordinates (r, φ), where $0 \le r \le R$, $0 \le \varphi \le 2\pi$, of the above-mentioned torsion-stressed $LiNbO_3$ crystalline element:

$$J_T=\left[\begin{array}{c|c}\cos(AMr)+i\sin(AMr)\cos(\varphi) & i\sin(AMr)\sin(\varphi)\\ \hline i\sin(AMr)\sin(\varphi) & \cos(AMr)-i\sin(AMr)\cos(\varphi)\end{array}\right]. \qquad (12)$$

3. Results and discussion

Optical systems of the elementary (single) cascades: T^{+-}, T^{++}, T^{-+} and T^{--}, are presented in Fig. 1. Here, the first superscript index sign indicates the sign of the outgoing wave's orbital angular momentum, while the second superscript index indicates the sign of the outgoing optical wave's circular polarization ("+" lefthanded, "-" righthanded).

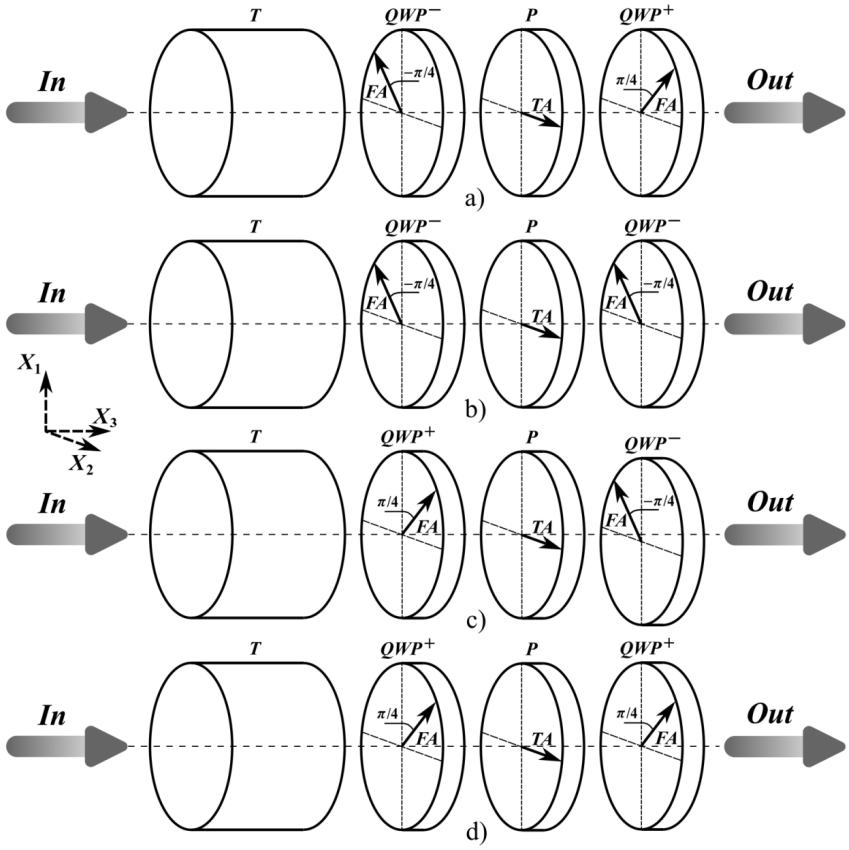

Fig. 1. Optical systems of single-cascades T^{+-} (a), T^{++} (b), T^{-+} (c), and T^{--} (d) for the torsion-stressed $LiNbO_3$ crystalline element *T*. QWP^+ and QWP^- are quarter-wave plates, the fast axes (*FA*) of which are located, respectively, at angles of $+\pi/4$ and $-\pi/4$ with respect to to the X_1 axis; *P* is a linear polarizer with a transmission axis (*TA*) parallel to the X_2 axis.

For single cascades T^{+-} (Fig. 1a) and T^{++} (Fig. 1b), we choose a left circularly polarized optical wave propagating along the optical axis of a twisted cylindrical $LiNbO_3$ crystalline sample as an input optical wave. The Jones vector of the electric field of this optical wave is determined by the relation

$$E_L = \frac{1}{\sqrt{2}}\begin{bmatrix} 1 \\ i \end{bmatrix}. \tag{13}$$

In the case under consideration, the Jones vectors of the electric field of the output optical waves for a single cascades T^{+-} and T^{++} are written, respectively, as

$$E_{out}^{+-} = J_{QWP^+} J_P J_{QWP^-} J_T E_L, \tag{14}$$

$$E_{out}^{++} = J_{QWP^-} J_P J_{QWP^-} J_T E_L, \tag{15}$$

where the Jones matrices QWP^+, QWP^- and P are, respectively,

$$J_{QWP^+} = \frac{1}{\sqrt{2}}\begin{bmatrix} 1 & i \\ i & 1 \end{bmatrix}, J_{QWP^-} = \frac{1}{\sqrt{2}}\begin{bmatrix} 1 & -i \\ -i & 1 \end{bmatrix}, J_P = \begin{bmatrix} 0 & 0 \\ 0 & 1 \end{bmatrix}. \tag{16}$$

After the appropriate matrix transformations of relations (14) and (15), we obtain the Jones vectors of the electric field of the output optical waves, which are determined, respectively, by the relations

$$E_{out}^{+-} = \sin(AMr)\exp(i(\varphi + \pi/2))E_R, \tag{17}$$

$$E_{out}^{++} = \sin(AMr)\exp(i(\varphi - \pi/2))E_L, \tag{18}$$

where E_R is the Jones vector of the electric field of a right circularly polarized optical wave:

$$E_R = \frac{1}{\sqrt{2}}\begin{bmatrix} 1 \\ -i \end{bmatrix}. \tag{19}$$

As can be seen, after passing through single cascades T^{+-} and T^{++}, the optical wave remains circularly polarized but acquires a radial distribution of intensity $\mathrm{I} \sim \sin^2(AMr)$ and a non-uniform phase delay $\Phi = l\varphi + \Phi_0$, where $l = 1$. Moreover, for the single cascade T^{+-}, the phase delay $\Phi_0 = \pi/2$ is introduced by the last quarter wave plate QWP^+, and for the single cascade T^{++} the phase delay $\Phi_0 = -\pi/2$ is introduced by the last quarter wave plate QWP^-. In addition, in the case of a single cascade T^{+-}, the optical wave changes the sign of circular polarization from left to right. Finally, when the incident optical wave has a left-handed circular polarization, the cascades T^{+-} and T^{++} generate a vortex beam with a charge equal to +1.

Instead, for single cascades T^{-+} (Fig. 1c) and T^{--} (Fig. 1d) we choose a right circularly polarized optical wave that propagates along the optical axis of a twisted cylindrical $LiNbO_3$ crystalline sample as an input optical wave. As indicated above, the Jones vector of the electric field of this optical wave E_R is determined by relation (19).

In turn, the Jones vectors of the electric field of the output optical waves for single cascades T^{-+} and T^{--} are equal, respectively, to

$$E_{out}^{-+} = J_{QWP^-} J_P J_{QWP^+} J_T E_R. \tag{20}$$

$$E_{out}^{--} = J_{QWP^+} J_P J_{QWP^+} J_T E_R. \tag{21}$$

After the appropriate matrix transformations of relations (20) and (21), we obtain the Jones vectors of the electric field of the output optical waves, which are determined, respectively, by the relations

$$E_{out}^{-+} = \sin(AMr)\exp(i(-\varphi + \pi/2))E_L. \tag{22}$$

$$E_{out}^{--} = \sin(AMr)\exp(i(-\varphi - \pi/2))E_R. \tag{23}$$

Thus, after passing through single cascades T^{-+} and T^{--}, the optical wave remains circularly polarized, but acquires a radial distribution of intensity $\mathrm{I} \sim \sin^2(AMr)$ and a non-uniform phase delay $\Phi = l\varphi + \Phi_0$, where $l = -1$. Wherein for the single cascade T^{-+}, the phase delay $\Phi_0 = \pi / 2$ is introduced by the last quarter wave plate QWP^- and for the single cascade T^{--} the phase delay $\Phi_0 = -\pi / 2$ is introduced by the last quarter wave plate QWP^+. In addition, in the case of a single cascade T^{-+}, the optical wave changes the sign of circular polarization from right to left. Finally, a single cascades T^{-+} and T^{--} generates a vortex beams with a charges equal to –1.

Taking into account the structure of relations (17), (18), (22), and (23), for N sequentially arranged single cascades of the above types, which use twisted cylindrical $LiNbO_3$ crystalline samples with the corresponding constants A_1, ..., A_N and the torque moments M_1, ..., M_N, at the output, a circularly polarized optical wave with a radial distribution of intensity $\mathrm{I} \sim \prod_{k=1}^{N} \sin^2(A_k M_k r)$ is obtained.

Let us consider the sequence of the different single cascades. It should be noted that when building such a multi-cascade optical system, the matching between adjacent single cascades must be ensured: the sign of the circular polarization of the output optical wave of the previous single cascade must coincide with the sign of the circular polarization of the input optical wave of the next single cascade. In this regard, we recall that after passing through single cascades T^{++} and T^{--}, the optical wave remains, respectively, left and right circularly polarized. In contrast, after passing through single cascades T^{+-} and T^{-+}, the sign of circular polarization changes, respectively, from left to right and from right to left.

(1) The sequence of cascades $T^{++}T^{++}$ lead to the transformation of the quantum state $|\sigma, l\rangle$ ($\sigma = \pm\hbar$ is the spin angular momentum) as $|\hbar, 0\rangle \Rightarrow |\hbar, 2\rangle$.

(2) The sequence of cascades $T^{--}T^{--}$ lead to the transformation of the quantum state as $|-\hbar, 0\rangle \Rightarrow |-\hbar, -2\rangle$.

(3) The sequence of cascades $T^{+-}T^{-+}$ lead to the transformation of the quantum state as $|\hbar, 0\rangle \Rightarrow |\hbar, 0\rangle$.

(4) The sequence of cascades $T^{-+}T^{+-}$ lead to the transformation of the quantum state as $|-\hbar, 0\rangle \Rightarrow |-\hbar, 0\rangle$.

(5) The sequence of cascades $T^{+-}T^{--}$ lead to the transformation of the quantum state as $|\hbar, 0\rangle \Rightarrow |-\hbar, 0\rangle$.

(6) The sequence of cascades $T^{-+}T^{++}$ lead to the transformation of the quantum state as $|-\hbar, 0\rangle \Rightarrow |\hbar, 0\rangle$.

In cases (1) and (2), using the multi-cascade optical system results in the multiplication of the orbital angular momentum. It is obvious that utilizing N cascades in these cases will lead to the generation of optical vortices with a charge equal to $\pm N$. In the third and fourth cases, the quantum state of the incident beam does not change. In the fifth and sixth cases, the quantum state changes, such as the spin angular momentum changes its sign, but an optical vortex is not generated.

Theoretical calculations of radial distributions of parameters $\mathrm{I} \sim \prod_{k=1}^{N} \sin^2(A_k M_k r)$ (Fig. 2) and

$\Phi - \Phi_0 = l\varphi$ (Fig. 3) for the output optical wave were carried out on the example of single-cascade and two-cascade optical systems (e.g. case (1) or (2)) according to the following data: $R = 3\times10^{-3}$ m, $d = 13\times10^{-3}$ m, $M = 63.77\times10^{-3}$ m×N [18], $n_0 = 2.28647$ [24], $\pi_{14} = 8.87\times10^{-13}$ m²×N⁻¹ [25], $\lambda = 632.8\times10^{-9}$ m.

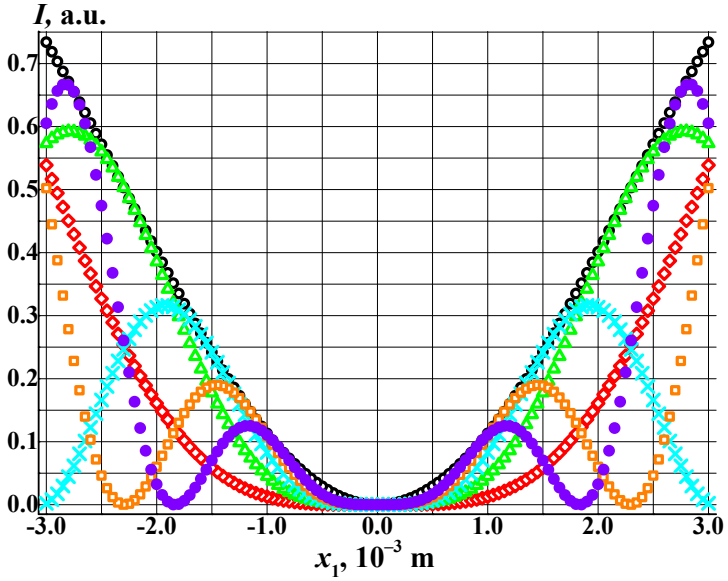

Fig. 2. Radial distribution of parameter I for the output optical wave in single-cascade optical systems (open circles) and two-cascade optical systems with $M_1 = M$, $M_2 = M$ (diamonds); $M_1 = M$, $M_2 = 2M$ (triangles); $M_1 = M$, $M_2 = 3M$ (crosses); $M_1 = M$, $M_2 = 4M$ (squares); $M_1 = M$, $M_2 = 5M$ (full circles).

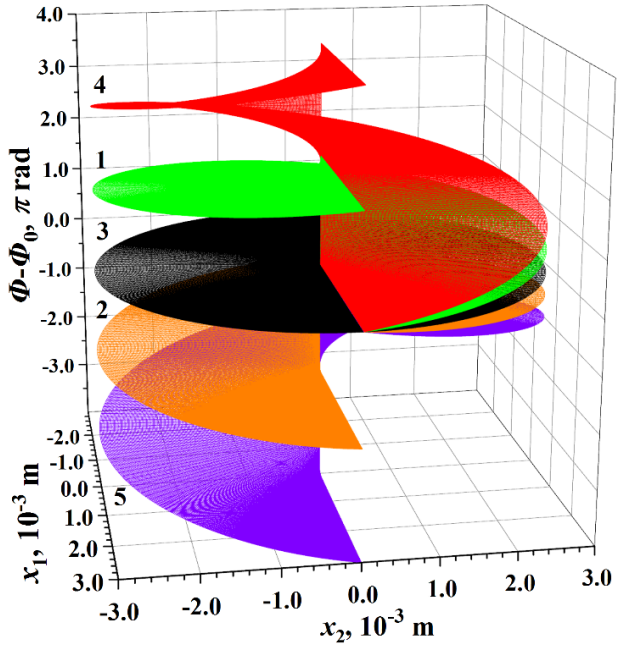

Fig. 3. Coordinate dependence of phase $\Phi - \Phi_0$ for the output optical wave in single-cascade optical systems with $l = +1$ (1), $l = -1$ (2) and two-cascade optical systems with $l = 0$ (3), $l = +2$ (4), $l = -2$ (5).

It is seen (Fig. 2) that at the chosen parameters, the single-cascade system does not produce a well-definite doughnut mode with a dark center and bright ring barrier. For this, increasing the torsion moment or the sample length is necessary. Nonetheless, the single-cascade configuration produces the single-charged optical vortex (Fig. 3). The two-cascade system can lead to the appearance of an optical beam, as Gaussian, as well as those that bear a double-charged vortex (Fig. 3). At the appropriate choice of torsion moment applied to different samples, e.g., $M_1 = M$, $M_2 = 3M$, one can generate a perfect, well-defined doughnut double-charged vortex beam with a bright single-ring barrier (Fig. 2). The cascade system presented in this work differs from the cascaded *q*-plates [14] by the existence in the Eqs. (17), (18), (22), and (23) and in the equation for the *N*-cascade system of the type multiplier $\sin^2(AMr)$, which permits one to operate by the parameters of the output beam by applying torsion moments (Figs. 2,3).

It should be noted that, with the aim of multiplexing, the generated vortex beams with defined charges can be deviated from the system using splitting optical elements for modulation and then mixed into one composite vortex beam for delivery at the receiver's side.

4. Conclusions

This work theoretically analyzed the possibility of generating vortices with different charges using multi-cascade optical systems that use torsion-stressed cylindrical $LiNbO_3$ crystalline elements. Thus, analytical relations were obtained for the Jones vectors of the electric field of the output optical wave in the case of four main types of elementary cascades. These allow for generating vortices with charges +1 and –1. It has been shown that with the help of only these four types of single cascades, when using the appropriate number of sequentially located cascades of one type, the generation of vortices with arbitrary integer charges can be realized. So, in particular, a two-cascade optical system allows the generating of optical vortices with charges –2, 0, and +2 depending on the number of cascades of a certain type. This approach can be easily implemented experimentally since it only combines torsion-stressed $LiNbO_3$ crystalline elements with quarter-wave plates and polarizers.

Moreover, to change the type of a certain defined single cascade, it is enough only to switch to the opposite diagonal orientation of the fast axes of the quarter-wave plates of this cascade. The cascade system presented in this work differs from the cascaded q-plates in terms of the possibility of operation by the outgoing beam parameters. This system can be used at the vortex beam multiplexing for information transfer.

Acknowledgement

The authors acknowledge the Ministry of Education and Science of Ukraine for financial support of this study (project #0124U000979).

References

1. Ren, Y., Wang, Z., Liao, P., Li, L., Xie, G., Huang, H., Zhao, Z., Yan, Y., Ahmed, N., Willner, A., Lavery, M. P. J., Ashrafi, N., Ashrafi, S., Bock, R., Tur, M., Djordjevic, I. B., Neifeld M. A. & Willner, A. E. (2016). Experimental characterization of a 400 Gbit/s orbital angular momentum multiplexed free-space optical link over 120 m. *Optics Letters*, *41*(3), 622-625.
2. Wang, J., Yang, J. Y., Fazal, I. M., Ahmed, N., Yan, Y., Huang, H., Ren, Y., Yue, Y., Dolinar, S., Tur M. & Willner, A. E. (2012). Terabit free-space data transmission employing orbital angular momentum multiplexing. *Nature Photonics*, *6*(7), 488-496.
3. Zhang, W., Li, Y., Sun, T., Shao, W., Zhu, F., & Wang, Y. (2016). Demodulation for multi vortex beams based on composite diffraction hologram. *Optics Communications*, *381*, 377-383.

4. Yang, C. H., Chen, Y. D., Wu, S. T., & Fuh, A. Y. G. (2016). Independent manipulation of topological charges and polarization patterns of optical vortices. *Scientific Reports*, *6*(1), 31546.
5. Qiao, Z., Wan, Z., Xie, G., Wang, J., Qian, L., & Fan, D. (2020). Multi-vortex laser enabling spatial and temporal encoding. *PhotoniX*, *1*, 1-14.
6. Zhu, L., & Wang, J. (2019). A review of multiple optical vortices generation: methods and applications. *Frontiers of Optoelectronics*, *12*, 52-68.
7. Du, J., & Wang, J. (2018). Dielectric metasurfaces enabling twisted light generation/detection/(de) multiplexing for data information transfer. *Optics Express*, *26*(10), 13183-13194.
8. Bazhenov, V. Y., Vasnetsov, M. V., & Soskin, M. S. (1990). Laser beams with screw dislocations in their wavefronts. *JEPT Lett*, *52*(8), 429-431.
9. Beijersbergen, M. W., Coerwinkel, R. P. C., Kristensen, M., & Woerdman, J. P. (1994). Helical-wavefront laser beams produced with a spiral phaseplate. *Optics Communications*, *112*(5-6), 321-327.
10. Marrucci, L., Manzo, C., & Paparo, D. (2006). Optical spin-to-orbital angular momentum conversion in inhomogeneous anisotropic media. *Physical Review Letters*, *96*(16), 163905.
11. Fadeyeva, T. A., Shvedov, V. G., Izdebskaya, Y. V., Volyar, A. V., Brasselet, E., Neshev, D. N., Desyatnikov, A.S., Krolikowski W. & Kivshar, Y. S. (2010). Spatially engineered polarization states and optical vortices in uniaxial crystals. *Optics Express*, *18*(10), 10848-10863.
12. Devlin, R. C., Ambrosio, A., Rubin, N. A., Mueller, J. B., & Capasso, F. (2017). Arbitrary spin-to–orbital angular momentum conversion of light. *Science*, *358*(6365), 896-901.
13. Ostrovsky, A. S., Rickenstorff-Parrao, C., & Arrizón, V. (2013). Generation of the "perfect" optical vortex using a liquid-crystal spatial light modulator. *Optics Letters*, *38*(4), 534-536.
14. Delaney, S., Sánchez-López, M. M., Moreno, I., & Davis, J. A. (2017). Arithmetic with q-plates. *Applied Optics*, *56*(3), 596-600.
15. Marrucci, L., Manzo, C., & Paparo, D. (2006). Pancharatnam-Berry phase optical elements for wave front shaping in the visible domain: Switchable helical mode generation. *Applied Physics Letters*, *88*(22).
16. Skab, I., Vasylkiv, Y., Savaryn, V., & Vlokh, R. (2011). Optical anisotropy induced by torsion stresses in $LiNbO_3$ crystals: appearance of an optical vortex. *JOSA A*, *28*(4), 633-640.
17. Skab, I., Vasylkiv, Y., Zapeka, B., Savaryn, V., & Vlokh, R. (2011). Appearance of singularities of optical fields under torsion of crystals containing threefold symmetry axes. *JOSA A*, *28*(7), 1331-1340.
18. Skab, I., Vasylkiv, Y., Smaga, I., & Vlokh, R. (2011). Spin-to-orbital momentum conversion via electro-optic Pockels effect in crystals. *Physical Review A*, *84*(4), 043815.
19. Skab, I., Vasylkiv, Y., Savaryn, V., & Vlokh, R. (2011). Optical anisotropy induced by torsion stresses in $LiNbO_3$ crystals: appearance of an optical vortex. *JOSA A*, *28*(4), 633-640.
20. Skab, I., Vasylkiv, Y., Zapeka, B., Savaryn, V., & Vlokh, R. (2011). Appearance of singularities of optical fields under torsion of crystals containing threefold symmetry axes. *JOSA A*, *28*(7), 1331-1340.
21. Piccirillo, B., D'Ambrosio, V., Slussarenko, S., Marrucci, L., & Santamato, E. (2010). Photon spin-to-orbital angular momentum conversion via an electrically tunable q-plate. *Applied Physics Letters*, *97*(24), 241104.
22. Sirotin, Y. and Shaskolskaya, M. (1983). *Fundamentals of Crystal Physics*. Imported Publications.
23. Gil, J. J., & Bernabeu, E. (1986). Obtainment of the polarizing and retardation parameters of a non-depolarizing optical system from the polar decomposition of its Mueller matrix. *Optik (Stuttgart)*, *76*(2), 67-71.
24. *Almaz Optics, Inc., Lithium niobate, $LiNbO_3$.* http://www.almazoptics.com/LiNbO3.htm.
25. Vasylkiv, Y., Savaryn, V., Smaga, I., Skab, I., & Vlokh, R. (2010). Determination of piezooptic coefficient π_{14} of $LiNbO_3$ crystals under torsion loading. *Ukrainian Journal of Physical Optics*, *11*(3), 156-164.

D. Adamenko, T. Kryvyy, I. Skab, and R. Vlokh. (2024). Optical Vortices Generated in Multi-Cascade Optical Systems with Torsion-Stressed $LiNbO_3$ Crystalline Elements. *Ukrainian Journal of Physical Optics*, *25*(2), 02099 – 02108.
doi: 10.3116/16091833/Ukr.J.Phys.Opt.2024.02099

Анотація. *У цій роботі теоретично перевірена можливість розширення спектру зарядів оптичних вихорів, створених за допомогою багатокаскадних оптичних систем на основі скручених навколо оптичної осі кристалів $LiNbO_3$. У результаті отримано аналітичні вирази для параметрів електричного поля вихідної оптичної хвилі для чотирьох основних типів елементарних каскадів, що дозволяють генерувати вихори із зарядами +1 та –1, а також забезпечують узгодження суміжних каскадів у*

мультикаскадній оптичній системі. При цьому було показано, що при використанні відповідної кількості послідовно розташованих каскадів, кожен з яких належить до певного типу з перерахованих вище, можна генерувати вихровий пучок з довільними цілими зарядами вихору, включаючи нуль. Використовуючи запропоновану каскадну систему, можна керувати параметрами вихідного променя. Цю систему можна використовувати при мультиплексуванні вихрового пучка для передачі інформації.

***Ключові слова**: оптичний вихор, гелікоїдальний хвильовий фронт, заряд вихора, багатокаскадна оптична система, крутильні напруження, кристали $LiNbO_3$.*